Persistent Quantum Coherence and Strong Coupling Enable Fast Electron Transfer across the CdS/TiO_2 Interface: A Time-Domain ab Initio Simulation

Hamid Mehdipour,[†] Alexey V. Akimov,[§] Joanna Jankowska,[||] Ali T. Rezakhanai,[†] Saeedeh S. Tafreshi,[†] Nora H. de Leeuw,[⊥] Alireza Z. Moshfegh,[*,†,‡] and Oleg V. Prezhdo[*,||]

[†]Department of Physics and [‡]Institute for Nanoscience and Nanotechnology, Sharif University of Technology, Tehran, Iran

[§]Department of Chemistry, University at Buffalo, The State University of New York, Buffalo, New York 14260-3000, United States [||]Department of Chemistry, University of Southern California, Los Angeles, California 90089, United States

[⊥]School of Chemistry, Cardiff University, Main Building, Park Place, Cardiff CF10 3AT, U.K.

[*] Supporting Information

ABSTRACT: Fast transfer of photoinduced electrons and subsequent slow electron−hole recombination in semiconductor heterostructures give rise to long-lived charge separation which is highly desirable for photocatalysis and photovoltaic applications. As a type II heterostructure, CdS/TiO_2 nanocomposites extend the absorption edge of the light spectrum to the visible range and demonstrate effective charge separation, resulting in more efficient conversion of solar energy to chemical energy. This improvement in performance is partly explained by the fact that CdS/TiO_2 is a type II semiconductor heterostructure and CdS has a smaller energy band gap than UV-active TiO_2. Ultrafast transient absorption measurements have revealed that electrons generated in CdS by visible light can quickly transfer into TiO_2 before recombination takes place within CdS. Here, using time-domain density functional theory and nonadiabatic molecular dynamics simulations, we show how electronic subsystems of the CdS and TiO_2 semiconductors are coupled to their lattice vibrations and coherently evolve, enabling effective transfer of photoinduced electrons from CdS into TiO_2. This very fast electron transfer, and subsequent slow recombination of the transferred electrons with the holes left in CdS, is verified experimentally through the proven efficient performance of CdS/TiO_2 heterostructures in photocatalysis and photovoltaic applications.

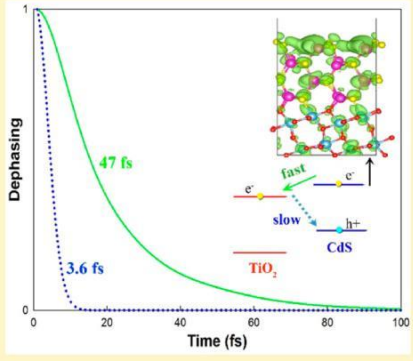

1. INTRODUCTION

Increasing environmental concerns over the extensive use of fossil fuels have led to research into the development of new technologies to convert solar energy into chemical and electric forms. Much attention has been dedicated to fabrication of solar-to-electricity/gas-conversion nanodevices based on semiconductor heterostructures.[1−4] In particular, heterostructures composed of metal oxides, such as TiO_2, are promising because they are abundant and photoresistive as well as chemically stable.[5−8] However, use of these materials is held back due to large band gaps (larger than 3 eV)[9] that can utilize only the very short-wavelength (near-UV) portion of the sunlight spectrum. Another drawback is effective charge carrier recombination, in which photoinduced electrons and holes recombine before they are well separated, which is required if they are to initiate photoreduction[10−14] or conduct an electric current.[4,15−18]

Making customized interfaces of different semiconductors can largely alleviate the disadvantages of isolated materials, e.g., the very low harvesting of visible light and high electron−hole recombination rates.[19] Small band gap semiconductors, such as CdS, CdSe, or related materials, can be used not only to improve the optical activity of TiO_2 and extend it to the visible range of the solar spectrum but also to enable effective charge separation in the semiconductor, thereby sufficiently increasing the lifetimes of photoinduced charges before they are lost as a result of recombination. The CdS-led visible activation of TiO_2 has been evidenced on numerous occasions by photoelectrochemical measurements, demonstrating high hydrogen generation rates for TiO_2 coupled to CdS under visible light illumination.[20−23] Similarly, for photovoltaic applications experimental measurements have shown a substantial increase in generated photocurrent for CdS-sensitized TiO_2 photoanodes exposed to solar light.[24−26] In addition to spectral improvement, these materials are thermally stable and photochemically robust, and combined with TiO_2 they provide highly durable heterostructures for photoconversion applications.

When TiO_2 is complemented by CdS, a type II electronic band alignment for the semiconductor heterostructure is formed. This enables an effective charge separation across the CdS/TiO_2 junction as a result of the thermally favorable injection of visible-light-excited electrons from the conduction band (CB) of CdS into the CB of TiO_2.[27] The electron transfer has been measured to be faster than the recombination of the photoelectrons and holes.[28−30] This fast transfer could reduce the recombination of the photoinduced charges, thus resulting in longer-lived photoinduced electrons, which is desirable for postseparation photoreduction processes.[20,21] However, the electron transfer efficiency could be reduced by other competitive electron loss pathways, such as electron− hole recombination across the interface or charge trapping on the surface of the semiconductor electron donor.[31,32]

Recently, synthesis of CdS/TiO_2 heterostructures with different morphologies, e.g., CdS quantum dots,[33,34] nanoparticles/nanotubes,[20,35] and core−shell forms,[29] has been reported. Ultrafast transient absorption (TA) spectroscopy measurements have shown fast transfer of photoexcited electrons across CdS/TiO_2 interfaces before the electron and hole recombine in CdS nanocrystals.[28,29] It has been also shown that the electron injection from the zinc-blende phase of CdS nanocrystals is remarkably faster than from the wurtzite phase.[29]

Here, using nonadiabatic molecular dynamics (NAMD) within the framework of time-dependent density functional theory (TDDFT), we have studied the dynamics of photoexcited charges in the CdS/TiO_2 heterostructure and made complete time-resolved comparisons of electron transfer (ET) and possible electron−hole recombination pathways across the CdS(110)/TiO_2(101) interface and inside each isolated semiconductor. This choice of the interface is based on HRTEM observations made by Zhang et al.,[36] who showed that CdS and CdSe layers form an interface of CdS(110)/TiO_2(101) with anatase TiO_2 layers. By quantifying interactions of quantum electronic subsystem and phonon vibrations of the CdS/TiO_2 interface, our NAMD calculations rationalize the results of recent experimental TA measurements[30] and provide very good qualitative comparison with results of some other works that report time-resolved measurements of hot carrier dynamics in CdS/TiO_2 junctions.[28,29] The computed electron transfer and recombination time scales are in good agreement with TA measurements of Mazumdar et al.,[30] and their relative orders of magnitude are consistent with recent experimental reports.[28,29]

Our study provides numerical evidence that both adiabatic and nonadiabatic mechanisms largely contribute to the fast ET from CdS into TiO_2.[37] The former mechanism is strongly dependent on delocalization of donor or acceptor orbitals, while the latter requires a high density of CB states for TiO_2 as well as some vibrational phonon modes to accommodate the energy released during the nonadiabatic cooling of the photoexcited electronic subsystem.

Two possible electron−hole recombination processes within CdS and across the CdS/TiO_2 interface have been resolved to take place over longer time periods, and these are in very good agreement with reported time scales from TA measurements.[28−30] The slow recombination across the junction is due to very weak nonadiabatic coupling (NAC) between associated two edge electronic states as well as extremely rapid loss of the quantum coherence between these states.

An absorbed photon in CdS excites an electron from the valence band (VB) into the CB forming a transient electronic state inside the CdS nanocrystal. After excitation of the CdS electronic state, the photoexcited electron can transfer either adiabatically, by passing over a transition state barrier, or nonadiabatically, by hopping between the donor and acceptor states, into the CB of TiO_2, causing charge separation. Following the adiabatic electron transfer, the electron trans-ferred diffuses into the TiO_2 bulk, relaxing to the bottom of the CB, while the energy released is accommodated into the crystal vibrations.

Before the ET process, the photoexcited electron can recombine with the hole generated in the VB. As a result of the recombination, both photoinduced charges are lost with the energy released as photon radiation or phonons into lattice vibrations. This is an undesirable event and is the main source of charge and energy loss in semiconductor materials used for photoelectrochemical and photovoltaic applications. Also, the transferred electrons in the CB of TiO_2 and the hole left in the VB of CdS can weakly attract each other, thus promoting a very ineffective recombination process, which is believed to be orders of magnitude slower than the primary electron transfer.[32]

The dynamics of photoinduced charges are simulated using a mixed quantum-classical approach with an implemented decoherence-induced surface hopping (DISH) scheme within the framework of the time-dependent density functional theory in the Kohn−Sham representation.[38] Keeping the quantum-mechanical picture of electrons, the ions are treated classically, and effects of their wave packet nature on the electronic states are accounted for by linear optical theory.[39] This approach has been broadly implemented in studies of the photoinduced charge dynamics across interfaces of various heterostructures, such as MoS_2/$MoSe_2$,[40] MoS_2/WS_2,[41] and CdSe/CdS.[42] Excellent agreement has been reported with results of sophisticated ultrafast time-resolved measurements because this approach provides a detailed description of the evolution of quantum electronic subsystems subject to the interaction with semiclassical crystal vibrations.[43,44]

2. SIMULATION METHODOLOGY

We use the mixed quantum-classical picture of electron−lattice vibration dynamics by implementing the classical path approximation (CPA) of the decoherence-induced surface hopping (DISH) technique[38,45,46] In this picture, the electronic system is treated quantum mechanically, while lattice vibrations are treated classically. The wave packet nature of atoms is taken into account by calculating the decoherence time for each pair of states according to a linear optic response formalism.[39] Hopping between potential energy surfaces occurs at the decoherence events which are manifested by a stochastic collapse of the electronic state wave function toward the adiabatic basis states.[38] This technique provides a detailed time-domain description of the electron−lattice vibration interactions at the atomic scale and has been successfully used to model electron−phonon dynamics in various systems.[42,47−54] The detailed description of the time-domain DFT and linear optic theory of decoherence time calculations can be found in the Supporting Information.

The atomic relaxation, electronic structure, and ground-state (adiabatic) MD were performed using the Quantum Espresso (QE) program, which implements plane-wave expansion of the periodic electron wave functions.[55] Nonlocal exchange-

correlation interactions of electrons were treated based on the generalized gradient approximation (GGA) as implemented in the Perdew−Burke−Ernzerhof (PBE) functional.[56] The electrostatic interactions of the ionic cores and the valence electrons were described by the projector-augmented wave (PAW) pseudopotentials.[57] The van der Waals interactions between the two semiconductors are taken into account by the semiempirical Grimme DFT-D2 method.[58]

The initially relaxed CdS/TiO_2 interface is thermalized using molecular dynamics (MD) with the Andersen thermostat at 300 K for 1 ps. Following the heating process, a 3.1 ps adiabatic MD simulation was performed in the microcanonical ensemble with 1 fs atomic time step, and the very first 200 steps were used to sample initial conditions for NAMD. The NAMD simulations were performed using DISH[38] as implemented within the PYthon eXtended Ab initio Dynamics (PYXAID) code[43, 44] under the approximation of neglecting the back-reaction. For each process, electron transfer or electron−hole recombination, 100 initial geometries were selected randomly to sample trajectories, and the nonadiabatic effects have been averaged over these trajectories. To achieve better convergence in some cases, 1000 initial conditions have been sampled from the first 2 ps of the trajectories, and the NA Hamiltonian matrix was iterated twice to achieve longer NAMD simulation time. Finally, to treat electronic transitions, 1000 random number sequences have been used to sample the surface hopping probabilities.

Unit cells of zinc-blende CdS and anatase TiO_2 were fully optimized, allowing both the cell parameters and atomic positions to relax until the forces and total energy changes became smaller than the corresponding thresholds. Such structures were then used to construct CdS(110)/TiO_2(101) supercells for the interface. Four-layer (2 × 2) CdS(110) and 10-layer (2 × 2) TiO_2(101) slabs with lattice mismatch of just under 7% were used, and an orthorhombic supercell with dimension of a = 8.0 and b = 10.9 Å was made (see Figure 1 and Figure S1 of the Supporting Information). For the size and coordinates of optimized CdS/TiO_2, TiO_2, and CdS structures, please refer to Tables S1−S3 of the Supporting Information. A vacuum space of 25 Å normal to the interface was created to avoid spurious interactions between the interface and its periodic images. The bottom atoms of the TiO_2 slab were kept fixed, and the rest of the atoms were relaxed until the forces became smaller than 0.02 eV/Å. The energy cutoff for expansion of the electron wave function was set to 612 eV (45 Ry) for all steps of the simulation. For time-consuming MD steps, the energy eigenvalues were calculated only at the gamma point, and a dense 8 × 8 × 1 Monkhorst−Pack mesh was used to compute more accurate partial densities of states of the interface at temperatures 0 and 300 K. More details of the simulation procedure and theory behind it can be found in the Supporting Information.

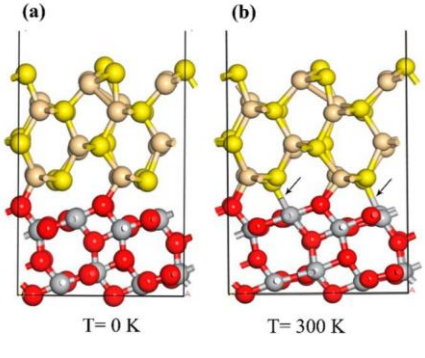

Figure 1. Geometries of the CdS(110)/TiO_2(101) interface at temperature (a) T = 0 K and (b) 300 K. The black arrows in (b) show the new bonds formed at the interface when atoms get closer to each other upon thermalization. Cd, S, Ti, and O atoms are denoted by wheat, yellow, gray, and red colors, respectively.

3. RESULTS AND DISCUSSION

3.1. Geometric and Electronic Structures of the CdS/TiO_2 Interface. Figure 1a shows the relaxed geometry of the CdS(110)/TiO_2(101) interface at 0 K. It is clearly seen that inter-semiconductor bonds are formed between O and Cd from TiO_2 and CdS, respectively. The average length of these relaxed Cd−O bonds is 2.34 Å, which is exactly the same as the Cd−O bond length in bulk cadmium oxide (2.34 Å), indicating a very strong interaction (binding) between the two semiconductors. The strong binding between donor and acceptor atoms suggests a notable delocalization of charge density distributions of corresponding electronic states. The strong binding could enable an effective adiabatic ET, which normally takes place at initial stages of electron excitation.[40] The figure also presents a snapshot of the interface from the MD trajectory at 300 K. It shows that at this higher temperature stronger interactions between the donor and acceptor materials are expected as a result of thermal motions of atoms of each semiconductor normal to the interface (see Figure S2). Therefore, one may expect stronger coupling between donor and acceptor electronic states which participate in the electron transfer process.

The projected density of states (PDOS) of each atom in the total density of states is shown in Figure 2a. The calculated PDOS's are for the relaxed interface at 0 K. It is clearly seen that a right type II band alignment with tangible lowest unoccupied molecular orbital (LUMO) offset is obtained for CdS and TiO_2. This band alignment is almost unchanged at room temperature (see Figure S3), which shows that the order of contributing states in the charge dynamics remains intact during the MD runs. The LUMO offset across the interface is almost 0.3 eV, which is an order of magnitude larger than the CdS exciton binding energy (28 meV),[59] indicating that the electron injection is also thermally favorable and that the excited electron can transfer partly nonadiabatically into TiO_2 by losing its energy into phonons. The 0.3 eV offset calculated for LUMOs of CdS and TiO_2 is consistent with the reported conduction edge offsets.[20, 34, 60] Similar LUMO offset values have also been calculated with DFT-based electronic band structure theory.[36]

GGA functionals can produce substantial errors in band gaps and lead to erroneous band edge alignments. However, in the present work, the GGA exchange-correlation theory has generated the right band edge alignment of type II, which is suitable for studying charge charger dynamics across the interface. When studying charge recombination, we have rescaled the band gaps to the more accurate values reported in experimental works. In addition, when an electron is excited from the valence band into the conduction band of a semiconductor, it is bound to the hole left in the valence band because of electrostatic attraction between the charges. Because the dielectric constant is high in semiconductors, the electron−hole distance is much larger than the lattice constant, and the electron−hole binding energies are small, falling within

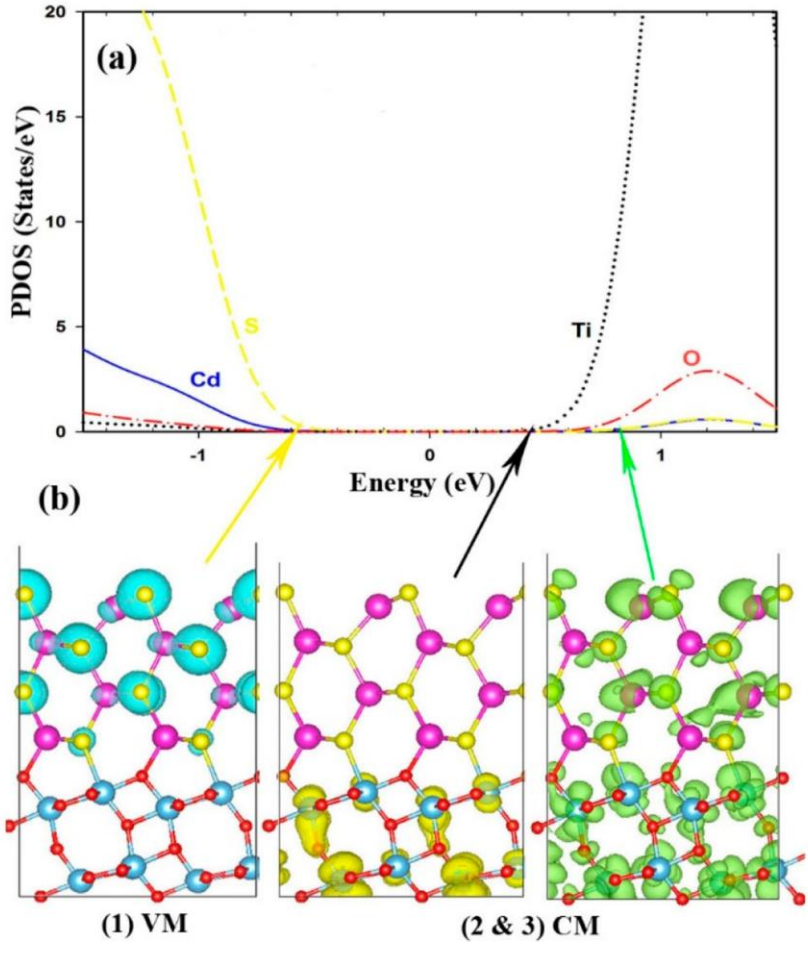

Figure 2. (a) Partial density of states of Cd (blue solid), S (yellow dashed), Ti (black dotted), and O (red dash-dotted) atoms in the CdS/TiO_2 heterostructure at temperature $T = 0$ K. The Fermi energy is set at zero. (b) Charge densities of the key band edge states at the interface: (1) HOMO of CdS and LUMO of (2) TiO_2 and (3) CdS.

a meV range. In particular, the measured exciton binding energies for CdS and TiO_2 are 28 meV[59] and 180 meV,[2] respectively. Accounting for exciton binding preserves the band alignment, since the TiO_2 energy level is decreased more than the CdS energy level.

In addition to underestimating band gaps, which can be corrected by gap scaling, GGA functionals produce more delocalized states, likely overestimating donor−acceptor coupling. At the same time, by underestimating the band edge offset, GGA functionals underestimate the density of acceptor states at the donor state energy, since densities of state generally increase with energy. These two errors tend to cancel each other. Increasing the simulated system size also has opposite effects on donor−acceptor coupling and density of states. As the system size increases, the density of acceptor states grows as well. At the same time, the donor−acceptor coupling decreases because electronic states delocalize away from the interface in a larger system and thus overlap less. The use of both more advanced DFT functionals and larger simulation cells demands great increased computational efforts.

PDOS calculations for each atom indicate that empty Ti 3d and filled S 3p orbitals largely constitute the LUMO and highest occupied molecular orbital (HOMO) of the semiconductor heterostructure, respectively. This can also be seen more clearly in the spatial charge density plots of the corresponding LUMO and HOMO energy levels (see Figure 2b), where the LUMO and HOMO charge densities are localized around Ti and S atoms, respectively.

It should be noted that the anatase TiO_2 is an indirect band gap semiconductor with energy band gap of ~3.1 eV. The indirect nature of the band gap slows down the recombination of electrons and holes that relaxed to the band edges. Our band structure calculation reveals that the composite system (CdS/TiO_2) has a direct band gap at the Γ-point (see Figure S6). The focus of the present works is on the dynamics of charge carriers in the combined system, and calculations of the electronic properties at the Γ-point calculation suffice to model the recombination dynamics across the interface. Using a denser sampling of the Brillouin zone introduces significant additional computational expense.

3.2. Electron Transfer and Electron−Hole Recombination. We have assumed that upon photoirradiation of CdS the electrons are instantaneously excited from valence bands into conduction bands. Following the photoexcitation, the electrons can undergo three processes: (1) either relaxing into the LUMO and then recombining with generated holes left in HOMO, (2) transferring to the nearby TiO_2 semiconductor and relaxing into the LUMO of TiO_2, and (3) the transferred electrons in TiO_2 can return into CdS and recombine with the left holes (see the energy level diagram in Figure 3).

To better understand the origin of charge separation at the CdS/TiO_2 junction, distributions of charge densities for donor

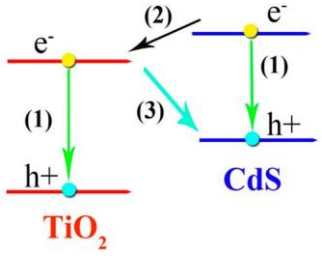

Figure 3. Schematic of electronic energy levels involved in the ET and electron−hole recombination at the CdS/TiO_2 interface and in pure CdS and TiO_2. Shown are the processes studied in the present work. (1) Photogenerated electrons and holes in pure CdS and TiO_2 can recombine, leading to loss of charge. (2) Photoexcited electron can undergo transfer across the interface. (3) The transferred electron in TiO_2 can recombine with the hole left in CdS.

and acceptor states have been shown in Figure 2b. The delocalization of donor and acceptor state wave functions can enable immediate transfer of photoinduced charge upon irradiation,[32,40,61] which could be much enhanced at higher temperatures, when thermal atomic vibrations provide larger overlap of donor and acceptor orbitals (see Figure S2). As is clearly seen in Figure 2, the S 3p and Ti 3d orbitals mainly form the donor and acceptor states, respectively. The delocalization of donor and acceptor orbitals is not particularly surprising, since the two semiconductors interact covalently with each other, whereas a higher density of states exists for the acceptor than for the donor state. This interaction is more pronounced at higher temperatures when thermalized atomic vibrations allow larger overlap of wave functions of contributing orbitals in the transfer process (Figure S2), which is clearly seen in Figure 1b, where Ti and S atoms are closer for the thermalized interface.

The delocalization of the donor state onto the acceptor material suggests that a strong overlap of corresponding wave functions exists for electron transfer (see Table 1), and as a result, a fraction of the photoexcited electron can be transferred, while an electron−hole pair is formed. Table 1 shows the calculated nonadiabatic coupling factor for electron transfer as well as the electron transition within TiO_2 CB. The NAC quantifies the strength of coupling between a pair of electronic states and how fast one changes in time with respect to the other. Based on these values, the nonadiabatic couplings of states belonging to the same material are expected to be much larger than the couplings belonging to the two complementary materials (Table 1). The relatively large averaged couplings (greater than 2.5 meV) between the donor and acceptor energy levels facilitate fast electron transfer dynamics across the heterostructured interface. The fast dynamics is assisted further by long coherence between the energy levels.

Table 1. Canonically Averaged Decoherence Times (DT) and Absolute Values of Nonadiabatic Coupling (NAC) for Pairs of States Belonging to TiO_2 and CdS

process	DT (fs)	NAC (meV)
LUMO(CdS)−LUMO(TiO_2)	47	3.73
LUMO+1(CdS)−LUMO(TiO_2)	36	3.40
LUMO+2(CdS)−LUMO(TiO_2)	26	2.96
LUMO(TiO_2)−LUMO+1(TiO_2)	103	10.00
LUMO(TiO_2)−LUMO+2(TiO_2)	73	5.11
LUMO(TiO_2)−LUMO+3(TiO_2)	63	3.11

The two processes studied here, electron transfer and electron−hole recombination, are governed by interactions between donor and acceptor electronic states as well as interactions between electronic states and atomic vibration modes of the system (electron−phonon interactions). The electron−phonon interactions are particularly important for nonradiative recombination of photoinduced electrons and holes in the system. For electron transfer, the earliest stages of the process can take place adiabatically through overlap of charge density distributions of two isoenergy states within the two adjacent materials. The adiabatically transferred electrons in the CB of TiO_2 then cool to the CB minimum, and the energy released is accommodated into lattice vibrations coupled to the electronic subsystem. The electron cooling transition prevents adiabatic back-transfer of separated electrons into the donor materials, thus enabling a long-lived separation of photoinduced charges. However, Coulombic interactions between the electron in the LUMO of TiO_2 and the hole left in the HOMO of CdS allow a new back-transfer channel for electron−hole recombination across the interface.

Electron−phonon interactions (scattering) can be divided into two categories, i.e., (1) elastic and (2) inelastic interactions. The elastic interactions randomize phases of the electronic states, resulting in loss of coherence between pairs of electronic states.[38,62] Longer coherence for a pair of states can gives rise to a fast transition between the states. For example, if a slow decoherence occurs between the donor and acceptor states, a very fast transfer process would be expected to take place, and vice versa. The inelastic scattering of electrons and phonons results in a release of phonon quanta, converting electronic energy to heat and stimulating vigorous motion of nuclei.[62]

The decoherence time for each pair of states is estimated by computing the pure-dephasing time for the two states within the framework of the optical response theory formalism.[39] In this theory, the phonon-induced dephasing time can be computed from the un-normalized autocorrelation function (un-ACF) of the fluctuation of the energy difference of the two electronic states along the nuclear trajectory, $C_{un}(t)$ (see the Supporting Information). ACF measures the correlation between electronic states and lattice vibration modes that couple to the quantum electronic subsystem.[62] Larger initial un-ACF as well as irregular asymmetry fluctuations over time results in a fast loss of coherence between two states. In fact, a large initial un-ACF indicates high magnitude of gap oscillations, while irregular and asymmetric oscillations give rise to very fast decoherence.[62] The change of ACF and thus the decoherence rate of electronic subsystems can originate from the symmetry of molecular structures of materials.[63] If the local symmetry of an atomic bonding pattern is broken by doping with light atoms or introducing defects into the system, high-frequency vibrations might emerge that could cause rapid loss of coherence.

The inset in Figure 4a shows the un-ACF for the electron transfer between two CdS and TiO_2 electronic states involved in the ET process. The small-amplitude un-ACF fluctuations that have emerged for the donor and acceptor energy states are not particularly irregular, and a very small initial value is recorded for un-ACF, which leads us to conclude that fluctuations in the energy difference of these state are not

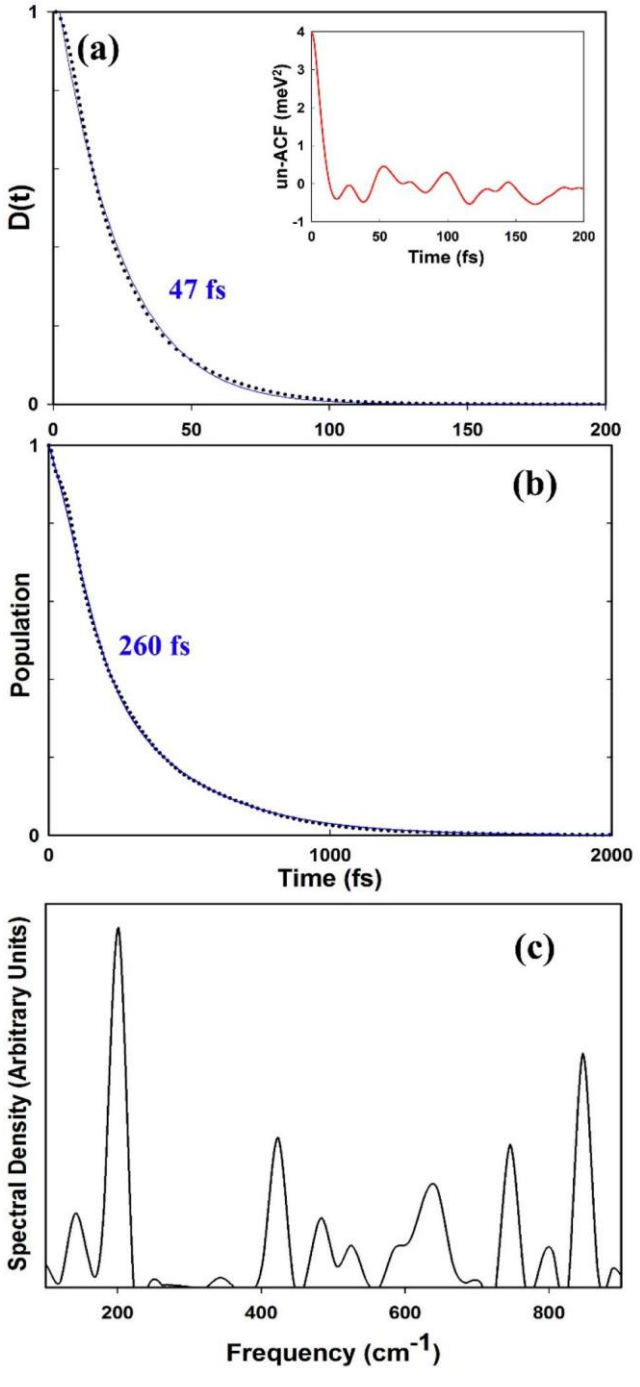

Figure 4. Dynamics of electron transfer across the CdS/TiO_2 interface. (a) Pure-dephasing function for the electron donor and acceptor orbital pair involved in the ET. The inset in (a) shows the corresponding un-normalized ACF. (b) Evolution of the donor state population. (c) Phonon influence spectrum contributing in the ET process. The results of fitting in (a) and (b) are shown with solid curves.

very large, and thus a long coherence between the two states over time would be expected.[62]

Gaussian decay is used to fit the pure-dephasing functions:

$$f(t) = \exp\left[-\frac{1}{2}\left(\frac{t}{t_g}\right)^2\right]$$

where t_g is the dephasing time constant. The pure-dephasing function is computed using the second-order cumulant approximation of the optical response theory, and Gaussian decay is appropriate for the fitting because it is can also be regarded as second order in time. The fitting results are presented in Table 1 for the electron relaxation and transfer processes (see Figure 4). Decoherence occurs faster for two states belonging to two complementary materials. In contrast, coherence is more persistent for states localized within the same material (see Table 1).

Figure 4a shows that the two donor and acceptor states oscillate coherently for a relatively long time (47 fs), despite the fact that the states involved in ET belong to the two semiconductors. This could be rationalized by covalent interaction between the two semiconductors and bonds formed between S and Ti atoms, as their orbitals mainly constitute the donor and acceptor orbitals. The long-living coherences ensure rapid transfer of photoexcited electrons, as has been highlighted in various systems from CdS into TiO_2, materializing as efficient charge separation in the CdS/TiO_2 heterostructure. It should be noted that the pronounced delocalization of orbitals and large overlaps between them results in large NACs, facilitating the transfer process. This effective interatomic interaction is more enhanced at room temperature (see Figure S2). This large NAC (3.7 meV), along with quantum coherence enhancement, makes charge transfer more effective across the interface.

The dynamics of the photoinduced charge separation and the subsequent relaxation are quantified in Figure 4b, where time evolution of population of CdS's LUMO orbital is displayed. The population is the ratio of number of trajectories in the excited state to total number of trajectories in the ensemble.[43] The LUMO orbital is initially occupied by the photoexcited electron, and its occupation number changes over time as it adibatically and nonadibatically couples to the host orbitals in the neighboring semiconductor (TiO_2). The time constants of the dynamics are obtained by fitting to the exponential decay $f(t) = \exp(-t/\tau)$. The calculated subpico-second transfer time, 260 fs, is consistent with transfer times measured by TA spectroscopy, 300−600 fs,[30] for the CdS/ TiO_2 heterostructure. The same fitting has been used for time evolution of the energies of the excited electrons transferring into TiO_2 (see Figure S4). The computed energy is with respect to the initial energy of the acceptor state. The NAMD computation shows that by accounting many near-edge excited states in the basis set, a relaxation time of 660 fs is obtained for the time evolution of excited-electron energies in the accessible high-density state CB manifold of the CdS/TiO_2 (see Figure S4).

Lattice vibrations in heterostructured semiconductors can promote charge separation and recombination between the semiconductors. They can accommodate the energy released as heat during these processes, which take place inside (or at the interface of) the semiconductors. Figure 4c shows the spectrum of lattice modes (influence spectrum) contributing to ET from CdS into TiO_2. The influence spectrum is calculated by FT of the energy offsets between the donor and acceptor states for the ET. The photoinduced electron in CdS couples to multiple phonon modes of both CdS and TiO_2. The dominant peaks that emerged can be attributed to low-frequency 199 cm^{-1} E_g phonon vibration of TiO_2[64] and high-frequency 600 cm^{-1} 2LO phonon vibration of CdS.[65] Another high-frequency phonon vibration of CdS 3LO,[66] which is the

second overtone of the fundamental optical 300 cm^{-1} mode, is seen that largely contributes to the ET process. The low-frequency E_g mode denotes O−Ti−O bending type vibration in the TiO_2 lattice.[64]

There are some peaks between the assigned peaks that could be overtones of main modes. These phonon modes might be artificial as a result of ensemble calculations. Among the contributing modes, the out-of-plane displacements of constituent atoms effectively influence the electron dynamics across the interface because these motions modulate energies of donor and acceptor states and change their coupling. It is not very surprising that both CdS and TiO_2 phonon modes contribute to the ET because both donor and acceptor states are partially delocalized across the interface (see Figure 2b). This spectrum of numerous phonon modes provides a strong coupling of lattice vibrations to the quantum electronic subsystem (large NAC) (see Table 2). This effectively speeds up the ET process, thus preventing charge loss (through recombination) within CdS. As a result, long-lived photo-induced electrons and holes are generated, which can then participate in the water oxidation and hydrogen reduction process.[20,21,67]

Table 2. Nonadiabatic Coupling (NAC) and Decoherence Time (DT) for Pairs of States Involved in Electron−Hole Recombination as Well as Calculated and Experimental Recombinatiom Time (RT) for Pure CdS, Pure TiO_2, and the CdS/TiO_2 Interface

	band gaps (rescaled, eV)	NAC (meV)	DT (fs)	RT (ps) (this work)	RT (ps) (expt)
CdS	1.6 (2.4)	1.380	56.0	1200	2700−3600[69,70]
TiO_2	3.3 (3.1)	0.952	12.3	3600	2300−6000[71,72]
CdS/ TiO_2	1.1	2.1	~4.0	~18	11−40[30]

When the electron transfers from CdS into the TiO_2, it still has an electrostatical interaction with the hole left in the VB of CdS. Therefore, the transferred electron can recombine with the hole leading to loss of charge and energy dissipation, which are undesirable phenomena in photoelectrochemical and solar energy applications. The charge recombination through the CdS/TiO_2 interface has been modeled by including edge states HOMO and LUMO as well as nearest-edge state HOMO−1, and LUMO+1, in the total basis set, to account for the role of near-edge states in thermally assisted transitions.

The details of the recombination dynamics are displayed in Figure 5. The inset in Figure 5a shows the un-ACF of the states involved in electron−hole recombination across the interface. The very large autocorrelation function at the beginning, as well as irregular and large-amplitude oscillations over time, suggests very brief coherent oscillation of involved energy states over time. This leads us to speculate that the very quick energy state dephasing would be expected for the contributing states in the energy state manifold of the recombination. The calculated ~4 fs dephasing time for the HOMO and LUMO states is a satisfying proof of the very short coherence maintained during the recombination process. Recombination occurs over a large energy range (nearly 1.0 eV, see Figure 2a), while energy transfer occurs over a small energy range of just 0.3 eV (see Figure S4). The decoherence effects are particularly important in the energy range of the recombination process because decoherence of energy states occurs much faster than the recombination, which could

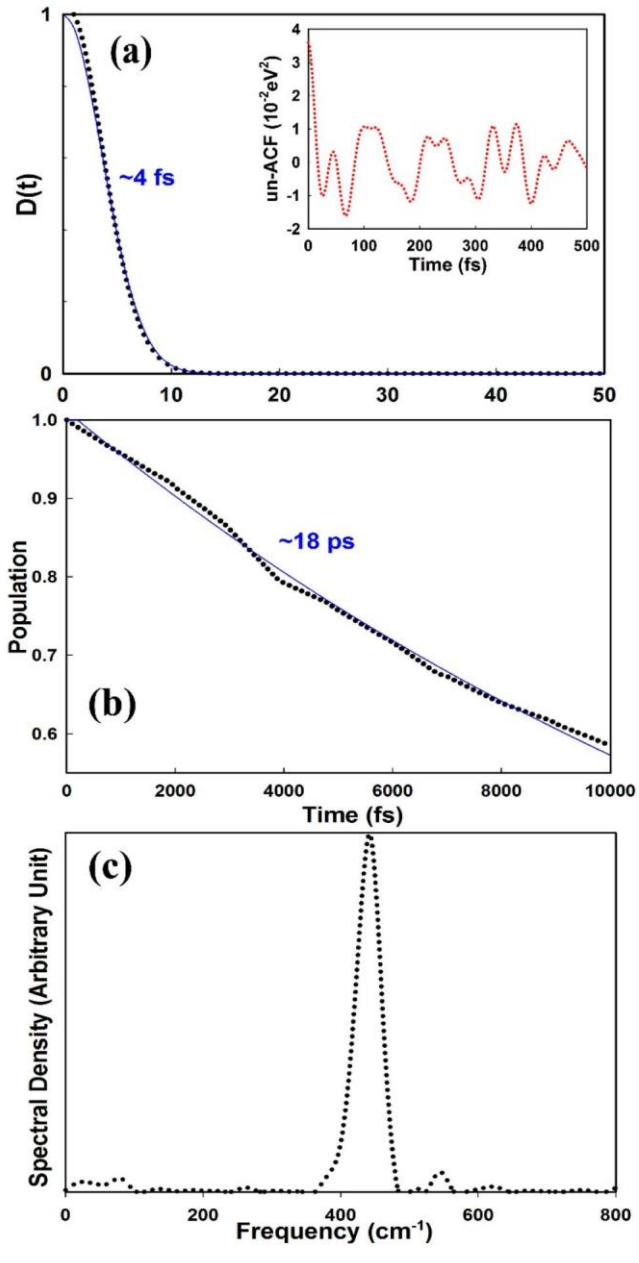

Figure 5. Dynamics of charge recombination across the CdS/TiO_2 junction: (a) Pure-dephasing function for the LUMO and HOMO state pair in the heterostructure involved in the recombination. The inset in (a) shows the corresponding un-normalized ACF. (b) Evolution of population of the LUMO of TiO_2. (c) Phonon influence spectrum for the charge recombination process. The results of fitting in (a) and (b) are shown with solid curves.

therefore slow the recombination. The quantified loss of coherence of the energy states (in shorter than 5 fs) could significantly slow the recombination process, although the nonadiabatic coupling between the states should be quantified to unravel the more effective factor in the overall quantum transition. Table 2 shows the NAC values obtained for states involved in recombination in the CdS/TiO_2 system as well as in pure CdS and TiO_2.

The calculated 18 ps recombination time is within the range of 11−40 ps reported for type II core−shell CdS/TiO_2 structures.[29] Inclusion of the near-edge states (HOMO−2 and LUMO+2) in the NAMD calculations changes the

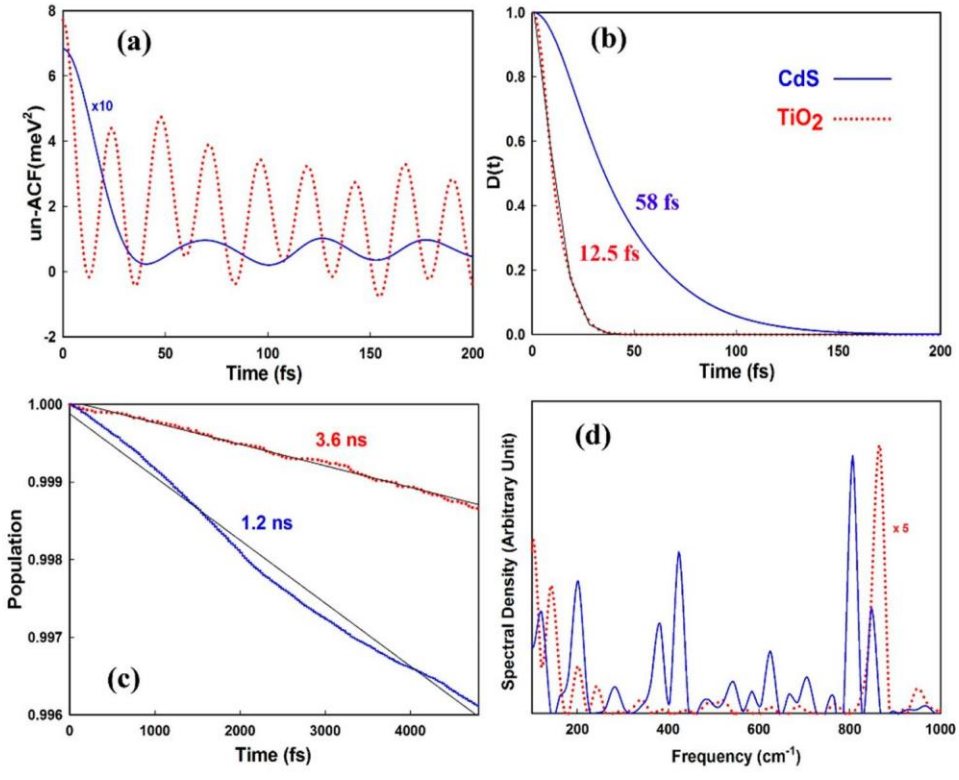

Figure 6. Dynamics of electron−hole recombination in isolated cubic CdS and anatase TiO_2, shown in blue and red, respectively. (a) Un-normalized ACF of the HOMO−LUMO energy gap. (b) Pure-dephasing function for the band gap (HOMO to LUMO) excitation. (c) Evolution of the excited state populations. (d) Phonon influence spectra. The un-ACF of CdS in (a) and the TiO_2 signal in (d) have been multiplied by 10 and 5, respectively.

recombination time only slightly (by 0.2 ps). The shorter transfer time reported in experiment could be due to structural defects (oxygen or sulfur vacancies) formed during the synthesis process. Such defects can enormously accelerate the electron transfer by forming unsaturated chemical bonds, and thus, by further extending the charge density of the S donor orbital onto the acceptor TiO_2 semiconductor, stronger donor−acceptor coupling occurs.

Given the short transfer time for the hot electrons across the interface, followed by the relatively slow recombination at the junction, one may conclude that the near-IR photoexcitation of the CdS/TiO_2 system would produce long-lived hot electrons and holes that could effectively participate in, for example, hydrogen reduction at TiO_2 and water oxidation at CdS, respectively. This enables an effective water-splitting process with greater absorption of the visible light spectrum, paving the way for customized materials design of photoelectrodes to fabricate efficient photoelectrochemical cells.

The nonradiative electron−hole recombination dynamics across the interface are primarily coupled to the 400 cm^{-1} B_{1g} vibration mode of TiO_2 (see Figure 5c). This mode, like the E_g mode, originates from the bending of O−Ti−O bonds in anatase TiO_2.[64,68] There are some other minor peaks around the main peak, though they are almost negligible in comparison. This very high intensity vibration coupled to the subspace of near-edge energy states accelerates decoherence of the energy states involved in the recombination dynamics.

We have also quantified the details of the recombination dynamics for pure CdS and TiO_2 semiconductors (see Figure 6). Figure 6a depicts the un-normalized ACF for both CdS and TiO_2. For CdS, a very small initial value of un-ACF is followed by regular small-amplitude oscillations, while for TiO_2 a larger initial un-ACF value is followed by regular large-amplitude oscillations. This suggests coherent oscillation of CdS recombination states over longer time periods and fast decoherence of recombination states in TiO_2. These are clearly seen in the computed dephasing function of the edge states for the two semiconductors; the loss of coherence take places much faster in TiO_2 than in CdS (see Figure 6b).

Figure 6c shows the evolution of populations of the LUMO states for the CdS and TiO_2 semiconductors. The computed recombination times of 1.2 and 3.6 ns for the zinc blende CdS and anatase TiO_2 structures (see Table 2) have the same order as of the experimentally determined time scales: 2.7−3.6 ns for CdS[69,70] and 2.3−6.0 ns for TiO_2.[71,72] The shorter recombination times measured for TiO_2 can be rationalized by the presence of common defects, such as O vacancies, inside the crystal structures. These defects create new states, so-called defect states, inside the band gap which can trap the hot charge carriers and thus accelerate the recombination.[47] The differ-ence in the recombination times for CdS/TiO_2 and pure CdS systems can be explained by the difference in the energy gaps involved. The recombination in CdS/TiO_2 occurs over a significantly smaller gap (1.1 eV) than in CdS (2.4 eV) (see also Table 2).

Figure 6d depicts the spectral densities of the energy gap for CdS and TiO_2 structures, characterizing the lattice vibration modes coupled to the recombination dynamics. The electronic subsystem of CdS couples primarily to the low-frequency 243 cm^{-1} E_1 (TO) and high-frequency 600 cm^{-1} overtone (2-LO)[73] and 800 cm^{-1} [74] of the CdS vibration modes. In TiO_2, the phonon modes of E_g (v_6) at 144 cm^{-1} mainly contribute to

the recombination. It should be noted that with respect to the TiO_2 recombination dynamics the slower loss of coherence for gap-edge states of CdS (Figure 6b) and stronger coupling between these two states (as a result of coupling to less intense vibrations) result synergistically in shorter recombination times in CdS. Considering the computed nanosecond time scale for recombination in CdS and very fast subpicosecond electron transfer across the CdS/TiO_2 junction, one can conclude that the charge separation can take place long before photoinduced charge can be recombined within the CdS semiconductor.

The computed time scales for charge dynamics studied in this work are highly consistent (in terms of order of magnitude) with time scales measured by sophisticated femtosecond laser-based optical methods. This is perhaps surprising since pure DFT methods (GGA) have been employed here without scaling of NAC parameters. Results from pure DFT methods, such as GGA, usually suffer from underestimation (for small unit cells) and overestimation (for large unit cells) of NACs, which could dramatically affect the computed charge dynamics times.[75]

4. CONCLUSIONS

Using time-domain density functional theory combined with nonadiabatic molecular dynamics, we have studied the photoinduced electron transfer and recombination dynamics at the CdS/TiO_2 interface as well as in pure CdS and TiO_2 semiconductors. The study explains why sophisticated transient absorption measurements demonstrate very fast charge separation for the CdS/TiO_2 heterostructures and effective photocatalytic activities observed in simple photoelectrochemical experiments. The charge separation is fast, since the donor and acceptor orbitals are delocalized into the acceptor and donor materials, respectively, the donor−acceptor interaction is very strong, and the quantum coherence between corresponding states is long-lived. The nonradiative electron−hole recombination across the interface is slow (2 orders of magnitude slower than the electron transfer), which indicates that separated charge carriers have long lifetimes and consequently can participate in oxidation and reduction processes before they are lost. This slow recombination can be attributed to rapid loss of coherence between the LUMO of TiO_2 and HOMO of CdS as a result of strong coupling of TiO_2 B_{1g} vibration modes to the quantum electronic subsystem. The results of the nonadiabatic molecular dynamics calculations are in good agreement with the time scales available from transient absorption spectroscopy measure-ments.

Given the nanosecond long lifetime of photoexcited electrons in CdS, the very short time for electron transfer across the CdS/TiO_2 interface, and long charge recombination time across the interface, one can conclude that charge separation in CdS/TiO_2 composites is very fast and long-lived, which could lead to very efficient photocatalytic and photovoltaic performances for this heterostructure, as already shown in a number of experiments.

ASSOCIATED CONTENT

* Supporting Information

Details of the nonadiabatic molecular dynamics methodology, including time-dependent density functional theory, fewest-switches surface hopping and decoherence induced surface hopping, views of the optimized system geometry, donor state charge densities, atom projected density of states, energy relaxation plot, and Cartesian coordinates of the optimized structures (PDF)

AUTHOR INFORMATION

Corresponding Authors

*E-mail prezhdo@usc.edu.

*E-mail moshfegh@sharif.edu.

ORCID

Alexey V. Akimov: 0000-0002-7815-3731

Joanna Jankowska: 0000-0002-7045-1478

Nora H. de Leeuw: 0000-0002-8271-0545

Alireza Z. Moshfegh: 0000-0003-3102-8906

Oleg V. Prezhdo: 0000-0002-5140-7500

Notes

The authors declare no competing financial interest.

ACKNOWLEDGMENTS

The authors thank the Research and Technology Council of Sharif University of Technology for support of the project. A.Z.M. acknowledges the Iran National Science Foundation (INSF) for its partial support (940006). H.M. thanks Navid Sarikhani for fruitful discussions and constructive comments on the work. This work has used computational facilities of the Advanced Research Computing @ Cardiff (ARCCA) Division, Cardiff University, UK. J.J. and O.V.P. acknowledge support of the U.S. National Science Foundation, Award CHE-1565704.

REFERENCES

(1) Wang, J.; Li, Y.; Deng, L.; Wei, N.; Weng, Y.; Dong, S.; Qi, D.; Qiu, J.; Chen, X.; Wu, T. High-Performance Photothermal Conversion of Narrow-Bandgap Ti_2O_3 Nanoparticles. Adv. Mater. 2017, 29, 1603730.

(2) Baldini, E.; et al. Strongly Bound Excitons in Anatase TiO_2 Single Crystals and Nanoparticles. Nat. Commun. 2017, 8, 13.

(3) Tang, Q. W.; Zhu, W. L.; He, B. L.; Yang, P. Z. Rapid Conversion from Carbohydrates to Large-Scale Carbon Quantum Dots for All-Weather Solar Cells. ACS Nano 2017, 11, 1540−1547.

(4) Seo, J.; Noh, J. H.; Seok, S. I. Rational Strategies for Efficient Perovskite Solar Cells. Acc. Chem. Res. 2016, 49, 562−572.

(5) Tian, J.; Zhao, Z. H.; Kumar, A.; Boughton, R. I.; Liu, H. Recent Progress in Design, Synthesis, and Applications of One-Dimensional TiO_2 Nanostructured Surface Heterostructures: A Review. Chem. Soc. Rev. 2014, 43, 6920−6937.

(6) Zhou, W. J.; Yin, Z. Y.; Du, Y. P.; Huang, X.; Zeng, Z. Y.; Fan, Z. X.; Liu, H.; Wang, J. Y.; Zhang, H. Synthesis of Few-Layer Mos2 Nanosheet-Coated TiO_2 Nanobelt Heterostructures for Enhanced Photocatalytic Activities. Small 2013, 9, 140−147.

(7) Zhang, J.; Bang, J. H.; Tang, C. C.; Kamat, P. V. Tailored TiO_2-$SrTiO_3$ Heterostructure Nanotube Arrays for Improved Photoelectrochemical Performance. ACS Nano 2010, 4, 387−395.

(8) Park, H.; Kim, H.-i.; Moon, G.-h.; Choi, W. Photoinduced Charge Transfer Processes in Solar Photocatalysis Based on Modified TiO_2. Energy Environ. Sci. 2016, 9, 411−433.

(9) Labat, F.; Baranek, P.; Domain, C.; Minot, C.; Adamo, C. Density Functional Theory Analysis of the Structural and Electronic Properties of TiO_2 Rutile and Anatase Polytypes: Performances of Different Exchange-Correlation Functionals. J. Chem. Phys. 2007, 126, 154703−1−13.

(10) Nozik, A. J. Photoelectrolysis of Water Using Semiconducting TiO_2 Crystals. Nature 1975, 257, 383−385.

(11) Varghese, O. K.; Paulose, M.; LaTempa, T. J.; Grimes, C. A. High-Rate Solar Photocatalytic Conversion of CO_2 and Water Vapor to Hydrocarbon Fuels. Nano Lett. 2009, 9, 731−737.
(12) Xu, W.; Jain, P. K.; Beberwyck, B. J.; Alivisatos, A. P. Probing Redox Photocatalysis of Trapped Electrons and Holes on Single Sb-Doped Titania Nanorod Surfaces. J. Am. Chem. Soc. 2012, 134, 3946− 9.
(13) Low, J.; Yu, J.; Jaroniec, M.; Wageh, S.; Al-Ghamdi, A. A. Heterojunction Photocatalysts. Adv. Mater. 2017, 29, 1601694.
(14) Guo, Q.; Zhou, C.; Ma, Z.; Ren, Z.; Fan, H.; Yang, X. Elementary Photocatalytic Chemistry on TiO_2 Surfaces. Chem. Soc. Rev. 2016, 45, 3701−3730.
(15) Lee, Y. H.; Luo, J.; Son, M. K.; Gao, P.; Cho, K. T.; Seo, J.; Zakeeruddin, S. M.; Gratzel, M.; Nazeeruddin, M. K. Enhanced Charge Collection with Passivation Layers in Perovskite Solar Cells. Adv. Mater. 2016, 28, 3966−72.
(16) Du, J.; et al. Zn-Cu-in-Se Quantum Dot Solar Cells with a Certified Power Conversion Efficiency of 11.6%. J. Am. Chem. Soc. 2016, 138, 4201−9.
(17) Zheng, L. X.; Han, S. C.; Liu, H.; Yu, P. P.; Fang, X. S. Hierarchical MoS2 Nanosheet@TiO_2 Nanotube Array Composites with Enhanced Photocatalytic and Photocurrent Performances. Small 2016, 12, 1527−1536.
(18) Roose, B.; Pathak, S.; Steiner, U. Doping of TiO_2 for Sensitized Solar Cells. Chem. Soc. Rev. 2015, 44, 8326−8349.
(19) Nijamudheen, A.; Akimov, A. V. Excited-State Dynamics in Two-Dimensional Heterostructures: Sir/TiO_2 and Ger/TiO_2 (R = H, Me) as Promising Photocatalysts. J. Phys. Chem. C 2017, 121, 6520− 6532.
(20) Yousefzadeh, S.; Faraji, M.; Nien, Y. T.; Moshfegh, A. Z. Cds Nanoparticle Sensitized Titanium Dioxide Decorated Graphene for Enhancing Visible Light Induced Photoanode. Appl. Surf. Sci. 2014, 320, 772−779.
(21) Sun, W. T.; Yu, Y.; Pan, H. Y.; Gao, X. F.; Chen, Q.; Peng, L. M. CdS Quantum Dots Sensitized TiO_2 Nanotube-Array Photo-electrodes. J. Am. Chem. Soc. 2008, 130, 1124−1125.
(22) Li, C. L.; Yuan, J. A.; Han, B. Y.; Jiang, L.; Shangguan, W. F. TiO_2 Nanotubes Incorporated with Cds for Photocatalytic Hydrogen Production from Splitting Water under Visible Light Irradiation. Int. J. Hydrogen Energy 2010, 35, 7073−7079.
(23) Baker, D. R.; Kamat, P. V. Photosensitization of TiO_2 Nanostructures with Cds Quantum Dots: Particulate Versus Tubular Support Architectures. Adv. Funct. Mater. 2009, 19, 805−811.
(24) Zhang, Q. X.; Guo, X. Z.; Huang, X. M.; Huang, S. Q.; Li, D. M.; Luo, Y. H.; Shen, Q.; Toyoda, T.; Meng, Q. B. Highly Efficient Cds/Cdse-Sensitized Solar Cells Controlled by the Structural Properties of Compact Porous TiO_2 Photoelectrodes. Phys. Chem. Chem. Phys. 2011, 13, 4659−4667.
(25) Zhao, D.; Yang, C. F. Recent Advances in the TiO_2/Cds Nanocomposite Used for Photocatalytic Hydrogen Production and Quantum-Dot-Sensitized Solar Cells. Renewable Sustainable Energy Rev. 2016, 54, 1048−1059.
(26) Wang, C. B.; Jiang, Z. F.; Wei, L.; Chen, Y. X.; Jiao, J.; Eastman, M.; Liu, H. Photosensitization of TiO_2 Nanorods with Cds Quantum Dots for Photovoltaic Applications: A Wet-Chemical Approach. Nano Energy 2012, 1, 440−447.
(27) Kim, H.-i.; Kim, J.; Kim, W.; Choi, W. Enhanced Photocatalytic and Photoelectrochemical Activity in the Ternary Hybrid of CdS/ TiO_2/WO_3 through the Cascadal Electron Transfer. J. Phys. Chem. C 2011, 115, 9797−9805.
(28) Evans, J. E.; Springer, K. W.; Zhang, J. Z. Femtosecond Studies of Interparticle Electron Transfer in a Coupled CdS−TiO_2 Colloidal System. J. Chem. Phys. 1994, 101, 6222−6225.
(29) Han, S.; Pu, Y.-C.; Zheng, L.; Zhang, J. Z.; Fang, X. Shell-Thickness Dependent Electron Transfer and Relaxation in Type-II Core−Shell CdS/TiO_2 Structures with Optimized Photoelectrochemical Performance. J. Mater. Chem. A 2015, 3, 22627−22635.
(30) Mazumdar, S.; Roy, K.; Srihari, V.; Umapathy, S.; Bhattacharyya, A. J. Probing Ultrafast Photoinduced Electron Transfer to TiO_2 from CdS Nanocrystals of Varying Crystallographic Phase Content. J. Phys. Chem. C 2015, 119, 17466−17473.
(31) Mora-Sero,I.; Gimenez, S.; Fabregat-Santiago, F.; Gomez, R.; Shen, Q.; Toyoda, T.; Bisquert, J. Recombination in Quantum Dot Sensitized Solar Cells. Acc. Chem. Res. 2009, 42, 1848−1857.
(32) Li, L.; Long, R.; Prezhdo, O. V. Charge Separation and Recombination in Two-Dimensional MoS_2/WS_2: Time-Domain Ab Initio Modeling. Chem. Mater. 2017, 29, 2466−2473.
(33) Xu, Y.-F.; Wu, W.-Q.; Rao, H.-S.; Chen, H.-Y.; Kuang, D.-B.; Su, C.-Y. CdS/CdSe Co-Sensitized TiO_2 Nanowire-Coated Hollow Spheres Exceeding 6% Photovoltaic Performance. Nano Energy 2015, 11, 621−630.
(34) Nakamura, R.; Makuta, S.; Tachibana, Y. Electron Injection Dynamics at the Silar Deposited CdS Quantum Dot/TiO_2 Interface. J. Phys. Chem. C 2015, 119, 20357−20362.
(35) Gao, X.-F.; Sun, W.-T.; Hu, Z.-D.; Ai, G.; Zhang, Y.-L.; Feng, S.; Li, F.; Peng, L.-M. An Efficient Method to Form Heterojunction CdS/TiO_2 Photoelectrodes Using Highly Ordered TiO_2 Nanotube Array Films. J. Phys. Chem. C 2009, 113, 20481−20485.
(36) Zhang, B.; Zheng, J.; Li, X.; Fang, Y.; Wang, L.-W.; Lin, Y.; Pan, F. Tuning Band Alignment by CdS Layers Using a Silar Method to Enhance TiO_2/CdS/CdSe Quantum-Dot Solar-Cell Performance. Chem. Commun. 2016, 52, 5706−5709.
(37) Schwartz, B. J.; Bittner, E. R.; Prezhdo, O. V.; Rossky, P. J. Quantum Decoherence and the Isotope Effect in Condensed Phase Nonadiabatic Molecular Dynamics Simulations. J. Chem. Phys. 1996, 104, 5942−5955.
(38) Jaeger, H. M.; Fischer, S.; Prezhdo, O. V. Decoherence-Induced Surface Hopping. J. Chem. Phys. 2012, 137, 22A545.
(39) Mukamel, S. Principles of Nonlinear Optical Spectroscopy; Oxford University Press: New York, 1999.
(40) Long, R.; Prezhdo, O. V. Quantum Coherence Facilitates Efficient Charge Separation at a MoS_2/$MoSe_2$ Van Der Waals Junction. Nano Lett. 2016, 16, 1996−2003.
(41) Hong, X.; Kim, J.; Shi, S. F.; Zhang, Y.; Jin, C.; Sun, Y.; Tongay, S.; Wu, J.; Zhang, Y.; Wang, F. Ultrafast Charge Transfer in Atomically Thin MoS_2/WS_2 Heterostructures. Nat. Nanotechnol. 2014, 9, 682−6.
(42) Dong, S.; Pal, S.; Lian, J.; Chan, Y.; Prezhdo, O. V.; Loh, Z. H. Sub-Picosecond Auger-Mediated Hole-Trapping Dynamics in Colloi-dal CdSe/CdS Core/Shell Nanoplatelets. ACS Nano 2016, 10, 9370− 9378.
(43) Akimov, A. V.; Prezhdo, O. V. The Pyxaid Program for Non-Adiabatic Molecular Dynamics in Condensed Matter Systems. J. Chem. Theory Comput. 2013, 9, 4959−72.
(44) Akimov, A. V.; Prezhdo, O. V. Advanced Capabilities of the Pyxaid Program: Integration Schemes, Decoherence Effects, Multi-excitonic States, and Field-Matter Interaction. J. Chem. Theory Comput. 2014, 10, 789−804.
(45) Granucci, G.; Persico, M. Critical Appraisal of the Fewest Switches Algorithm for Surface Hopping. J. Chem. Phys. 2007, 126, 134114.
(46) Tully, J. C. Molecular Dynamics with Electronic Transitions. J. Chem. Phys. 1990, 93, 1061−1071.
(47) Zhou, Z.; Liu, J.; Long, R.; Li, L.; Guo, L.; Prezhdo, O. V. Control of Charge Carriers Trapping and Relaxation in Hematite by Oxygen Vacancy Charge: Ab Initio Non-Adiabatic Molecular Dynamics. J. Am. Chem. Soc. 2017, 139, 6707−6717.
(48) Jaeger, H. M.; Green, J. R.; Prezhdo, O. V. Decoherence Reduces Thermal Energy Loss in Graphene Quantum Dots. Appl. Phys. Lett. 2013, 103, 073111−1−13.
(49) Long, R.; English, N. J.; Prezhdo, O. V. Defects Are Needed for Fast Photo-Induced Electron Transfer from a Nanocrystal to a Molecule: Time-Domain Ab Initio Analysis. J. Am. Chem. Soc. 2013, 135, 18892−18900.
(50) Tafen, D. N.; Long, R.; Prezhdo, O. V. Dimensionality of Nanoscale TiO_2 Determines the Mechanism of Photoinduced Electron Injection from a CdSe Nanoparticle. Nano Lett. 2014, 14, 1790.

(51) Long, R.; Prezhdo, O. V. Dopants Control Electron−Hole Recombination at Perovskite−TiO_2 Interfaces: Ab Initio Time-Domain Study. ACS Nano 2015, 9, 11143−11155.
(52) Chaban, V. V.; Pal, S.; Prezhdo, O. V. Laser-Induced Explosion of Nitrated Carbon Nanotubes: Nonadiabatic and Reactive Molecular Dynamics Simulations. J. Am. Chem. Soc. 2016, 138, 15927−15934.
(53) Habenicht, B. F.; Prezhdo, O. V. Nonradiative Quenching of Fluorescence in a Semiconducting Carbon Nanotube: A Time-Domain Ab Initio Study. Phys. Rev. Lett. 2008, 100, 197402.
(54) Zhang, Z.; Fang, W. H.; Tokina, M. V.; Long, R.; Prezhdo, O. V. Rapid Decoherence Suppresses Charge Recombination in Multi-Layer 2D Halide Perovskites: Time-Domain Ab Initio Analysis. Nano Lett. 2018, 18, 2459−2466.
(55) Giannozzi, P.; et al. Quantum Espresso: A Modular and Open-Source Software Project for Quantum Simulations of Materials. J. Phys.: Condens. Matter 2009, 21, 395502−1−19.
(56) Perdew, J. P.; Burke, K.; Ernzerhof, M. Generalized Gradient Approximation Made Simple. Phys. Rev. Lett. 1996, 77, 3865−3868.
(57) Kresse, G.; Joubert, D. From Ultrasoft Pseudopotentials to the Projector Augmented-Wave Method. Phys. Rev. B: Condens. Matter Mater. Phys. 1999, 59, 1758−1775.
(58) Grimme, S. Semiempirical Gga-Type Density Functional Constructed with a Long-Range Dispersion Correction. J. Comput. Chem. 2006, 27, 1787−99.
(59) Ip, K. M.; Wang, C. R.; Li, Q.; Hark, S. K. Excitons and Surface Luminescence of CdS Nanoribbons. Appl. Phys. Lett. 2004, 84, 795− 797.
(60) Pan, X.; Xu, Y.-J. Graphene-Templated Bottom-up Fabrication of Ultralarge Binary CdS-TiO_2 Nanosheets for Photocatalytic Selective Reduction. J. Phys. Chem. C 2015, 119, 7184−7194.
(61) Long, R.; Fang, W.; Akimov, A. V. Nonradiative Electron−Hole Recombination Rate Is Greatly Reduced by Defects in Monolayer Black Phosphorus: Ab Initio Time Domain Study. J. Phys. Chem. Lett. 2016, 7, 653−659.
(62) Akimov, A. V.; Prezhdo, O. V. Persistent Electronic Coherence Despite Rapid Loss of Electron−Nuclear Correlation. J. Phys. Chem. Lett. 2013, 4, 3857−3864.
(63) Nijamudheen, A.; Akimov, A. V. Criticality of Symmetry in Rational Design of Chalcogenide Perovskites. J. Phys. Chem. Lett. 2018, 9, 248−257.
(64) Ohsaka, T.; Izumi, F.; Fujiki, Y. Raman Spectrum of Anatase, TiO_2. J. Raman Spectrosc. 1978, 7, 321−324.
(65) Diwate, K.; et al. Substrate Temperature Dependent Studies on Properties of Chemical Spray Pyrolysis Deposited CdS Thin Films for Solar Cell Applications. J. Semicond. 2017, 38, 023001−1−10.
(66) Kumar, P.; Saxena, N.; Chandra, R.; Gupta, V.; Agarwal, A.; Kanjilal, D. Nanotwinning and Structural Phase Transition in CdS Quantum Dots. Nanoscale Res. Lett. 2012, 7, 584−1−7.
(67) White, J. C.; Dutta, P. K. Assembly of Nanoparticles in Zeolite Y for the Photocatalytic Generation of Hydrogen from Water. J. Phys. Chem. C 2011, 115, 2938−2947.
(68) Zhang, W. F.; He, Y. L.; Zhang, M. S.; Yin, Z.; Chen, Q. Raman Scattering Study on Anatase Tio 2 Nanocrystals. J. Phys. D: Appl. Phys. 2000, 33, 912−916.
(69) Boiko, G. A.; Dneprovskii, V. S.; Kraevskii, M. V.; Marinova, K.; Oak, S. M.; Silina, E. K.; Fokin, V. S. A Study of the Kinetics of Recombination Radiation of CdS and CdSe Crystals. Phys. Status Solidi B 1978, 85, 111−119.
(70) Li, H. P.; Kam, C. H.; Lam, Y. L.; Ji, W. Optical Nonlinearities and Photo-Excited Carrier Lifetime in Cds at 532 Nm. Opt. Commun. 2001, 190, 351−356.
(71) Yamada, Y.; Kanemitsu, Y. Determination of Electron and Hole Lifetimes of Rutile and Anatase TiO_2 Single Crystals. Appl. Phys. Lett. 2012, 101, 133907−1−3.
(72) Pendlebury, S. R.; Wang, X.; Le Formal, F.; Cornuz, M.; Kafizas, A.; Tilley, S. D.; Gratzel, M.; Durrant, J. R. Ultrafast Charge Carrier Recombination and Trapping in Hematite Photoanodes under Applied Bias. J. Am. Chem. Soc. 2014, 136, 9854−7.
(73) Jiang, N.; Xiu, Z.; Xie, Z.; Li, H.; Zhao, G.; Wang, W.; Wu, Y.; Hao, X. Reduced Graphene Oxide−Cds Nanocomposites with Enhanced Visible-Light Photoactivity Synthesized Using Ionic-Liquid Precursors. New J. Chem. 2014, 38, 4312−4320.
(74) Tang, Y.; Liu, X.; Ma, C.; Zhou, M.; Huo, P.; Yu, L.; Pan, J.; Shi, W.; Yan, Y. Enhanced Photocatalytic Degradation of Tetracycline Antibiotics by Reduced Graphene Oxide−CdS/ZnS Heterostructure Photocatalysts. New J. Chem. 2015, 39, 5150−5160.
(75) Lin, Y.; Akimov, A. V. Dependence of Nonadiabatic Couplings with Kohn-Sham Orbitals on the Choice of Density Functional: Pure vs Hybrid. J. Phys. Chem. A 2016, 120, 9028−9041.